Palaeogeography, Palaeoclimatology, Palaeoecology 626 (2023) 111695

Contents lists available at ScienceDirect

Palaeogeography, Palaeoclimatology, Palaeoecology

journal homepage: www.elsevier.com/locate/palaeo

Cosmogenic nuclide chronological constraints on the late Cenozoic strata of the Linxia Basin, northeast Tibetan Plateau

Yu Liu [a,b], Lu Sun [c], Sheng Xu [d], Yan Ma [e], Ping Liu [f], Shijie Wang [a,b], Weijun Luo [a,b,*]

[a] State Key Laboratory of Environmental Geochemistry, Institute of Geochemistry, Chinese Academy of Sciences, Guiyang 550081, China
[b] Puding Karst Ecosystem Research Station, Chinese Academy of Sciences, Puding 562100, China
[c] School of Earth Science, East China University of Technology, Nanchang, Jiangxi 330013, China
[d] Institute of Surface-Earth System Science, Tianjin University, Tianjin 300072, China
[e] State Key Laboratory of Earthquake Dynamics, Institute of Geology, China Earthquake Administration, Beijing 100029, China
[f] College of Earth and Planetary Sciences, University of Chinese Academy of Scienc7es, Beijing 100049, China

ARTICLE INFO

Editor: H Falcon-Lang

Keywords:
Cosmogenic nuclide
Burial dating
Late Cenozoic
Linxia Basin
NE Tibetan Plateau

ABSTRACT

The thick Cenozoic sedimentary sequence of the Linxia Basin contains abundant well-preserved mammalian fossils, which provide significant information on the paleoenvironmental processes and mammalian evolution associated with the uplift and expansion of the Tibetan Plateau. Ambiguous age estimations have been made for some coarse-grained sedimentary units in the basin, which have led to the misinterpretation of biostratigraphic and magnetostratigraphic age models. To resolve these issues, we present radiometric dating of three late Cenozoic sedimentary units ("Liushu", Hewangjia, and Jishi formations) in the eastern Linxia Basin using cosmogenic $^{26}Al/^{10}Be$ and $^{10}Be/^{21}Ne$ burial methods. isotope measurements for the upper "Liushu" Formation indicate a $^{10}Be/^{21}Ne$ burial age of 11.70 ± 0.17 Ma. This age is older than, but not contrary to, recently revised bio-magnetostratigraphic work. The $^{26}Al/^{10}Be$ burial age of the Hewangjia Formation is 3.06 (+0.36/−0.31) Ma and had been underestimated by post-burial muon production possibility, while the $^{26}Al/^{10}Be$ burial age of the Jishi Formation is 2.50 (+0.20/−0.18) Ma and had been overestimated due to inherited cosmogenic nuclides from recycled deposits. The new age from the Jishi Formation delays the initial deposition of conglomerates in the Linxia Basin to no earlier than 2.5 Ma and constrains an important episode of tectonic uplift of the northeastern Tibetan Plateau to 2.5–3.1 Ma. The age of the *Equus* fauna of Longdan is revised to the Early Quaternary (ca. 2.1–1.9 Ma). Our new age determinations significantly refine the terrestrial sequence chronology of the Linxia Basin and associated mammalian faunas of the late Miocene to the early Pleistocene.

1. Introduction

The uplift and expansion of the Tibetan Plateau as a result of the India-Asia collision and convergence are among the most profound geological events in the Cenozoic. Hence, the associated lithospheric deformation mechanism and atmospheric circulation are among the most interesting topics in geosciences (e.g. Molnar et al., 1993; Tapponnier et al., 2001; An et al., 2001; Yuan et al., 2022). The northeastern margin of the plateau is a critical area for exploring the regional tectonism, topography, Asian monsoon system, Asian biodiversity, and the links between them (Fang et al., 2003; Garzione et al., 2005; Deng et al., 2013a; Miao et al., 2013; Zan et al., 2016; Zhang et al., 2020). This part of the Tibetan Plateau is characterized by a series of orogenic belts and sedimentary basins that are controlled by large folds, strike-slip faults, and thrust fault systems. The continuous infilling deposits documented in the sedimentary basin record a history of the adjacent orogen uplift, regional tectonic deformation history, and paleoenvironmental change (Deng et al., 2013a; Fang et al., 2003, 2016; Zan et al., 2016, 2018; Zhang et al., 2019, 2020).

The Linxia Basin belongs to an intermontane continental basin that lies on the northeastern rim of the Tibetan Plateau (Fig. 1A), which provides vital insights into the tectonic uplift of the West Qinling Shan (mountain) and the climate change in interior East Asia in the Cenozoic. The Cenozoic sediments within the basin are ~2000 m thick and comprise eolian, fluvial, and lacustrine sediments, of which some are indicative of freshwater and some of saline conditions. Such a thick and generally continuous sedimentary sequence with abundant terrestrial mammalian faunas in the basin records the mammalian and

* Corresponding author at: State Key Laboratory of Environmental Geochemistry, Institute of Geochemistry, Chinese Academy of Sciences, Guiyang 550081, China.
E-mail address: luoweijun@mail.gyig.ac.cn (W. Luo).

https://doi.org/10.1016/j.palaeo.2023.111695
Received 22 August 2022; Received in revised form 25 May 2023; Accepted 16 June 2023
Available online 25 June 2023

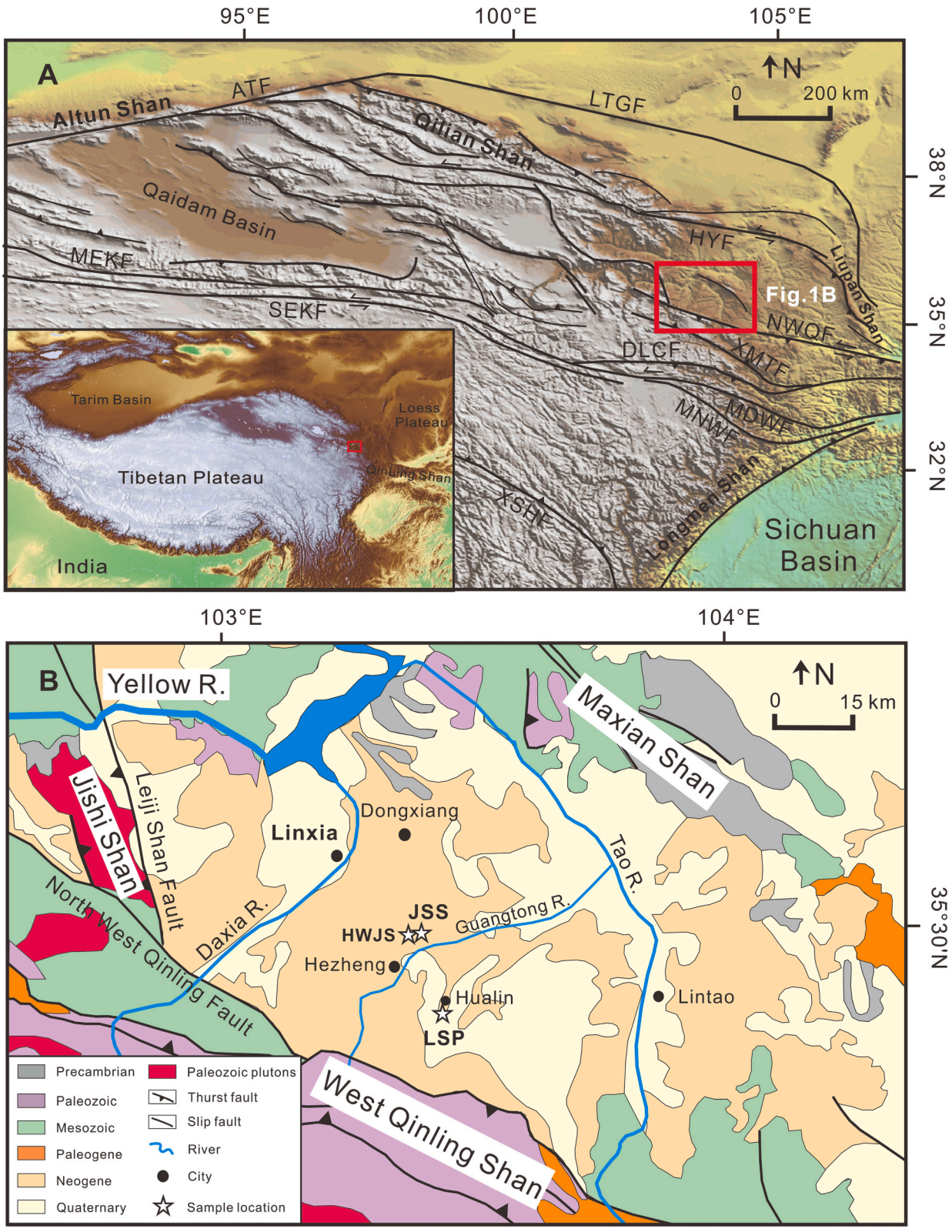

Fig. 1. (A) Digital elevation model image with a superimposed simplified tectonic map showing the location of the Linxia Basin on the northeastern margin of the Tibetan Plateau. ATF: Altyn Tagh Fault; DMF: Danghe-nanshan-Muli Fault; NQF: North Qilian Fault; ZWLF: Zongwulong Shan Fault; LTGF: Longshoushan-Tongxin-Guyuan Fault; HYF: Haiyuan Fault; TLSF: Tuolai Shan Fault; NEKF: North East Kunlun Fault; MEKF: Middle East Kunlun Fault; SEKF: South East Kunlun Fault; NWQF: North West Qinling Fault; XSHF: Xianshui He Fault; XMTF: Xiahe-Minxian-Tachang Fault; DLCF: Dieshan-Lazikou-Chengxian Fault; MDWF: Maqu-Diebu-Wudu Fault; MNWF: Maqu-Nanping-Wenxian Fault. (B) Geological map of the Linxia Basin showing the sampling sites (modified from Fang et al., 2016). Labeling of sample acronyms as used in Table 1.

environmental evolution associated with the stepwise uplift and northeastward expansion of the Tibetan Plateau since the late Paleogene.

The earliest geochronologic work in the Linxia Basin dates back to the middle of the 20th century. In 1965, the Cenozoic stratigraphy was first named the Linxia Group and subdivided into four formations based on the *Hipparion* fossils found in the geological investigation. They were the Oligocene Guyuan Formation, the Miocene Xianshuihe Formation, the Pliocene Linxia Formation, and the Quaternary Wangjiashan Formation (Gansu Geological and Mineral Resources Bureau, 1989). Beginning in the 1990s, Li et al. (1995) and Fang et al. (2003) resubdivided the Cenozoic stratigraphy of the Linxia Basin into eight formations based on lithofacies, contacts, magnetostratigraphy, and paleontology, as shown in Fig. 2. Six typical sections were studied using various dating methods, including magnetic stratigraphy, fission track of secondary gypsum, and amino acid racemization of lamellibranch and trees, to provide the chronology of the Cenozoic succession. Magnetic stratigraphy provides perhaps the most reliable chronology for the whole sequence, showing that the Linxia Basin began to accumulate by ca. 29 Ma (Li et al., 1995; Fang et al., 1997, 2003).

There are numerous mammalian fossils from several horizons within the Linxia Basin (Fig. 2). Four typical mammalian faunas, namely, the late Oligocene *Dzungariotherium* fauna, the middle Miocene *Platybelodon* fauna, the late Miocene *Hipparion* fauna, and the early Pleistocene *Equus* fauna, are mainly included, showing deteriorative ecological environment changes (Deng et al., 2004, 2013a). Each fauna has a representative fossil component that lived at a specific time, which gives a general chronological estimation of the fossiliferous layer accordingly, and all of them were correlated to the European mammal zones (Deng et al., 2004, 2013a). However, some conflicts existed between the age determinations of certain stratigraphic units by fossil mammals and magnetic polarity stratigraphies (Fig. 2; Qiu et al., 2004a; Deng et al., 2004; Fang et al., 2016). Divergence mainly existed in strata between the Oligocene and Miocene, and biochronology suggested an older chronological framework than magnetostratigraphic studies (Fig. 2). Deng et al. (2013a) argued that Li et al. (1995) and Fang et al. (1997, 2003) misallocated fossil horizons with consequent errors in the interpretation of magnetostratigraphy. Fang et al. (2016) assumed that the great diachroneity of stratigraphy in the Linxia Basin could explain the contradiction and debate on magnetostratigraphy and fossil mammals. Indeed, most of the fossil mammals were not found directly in the paleomagnetically dated sections in the previous work, resulting in an inevitable conflict. Consequently, Deng et al. (2013a) revised the lithostratigraphic

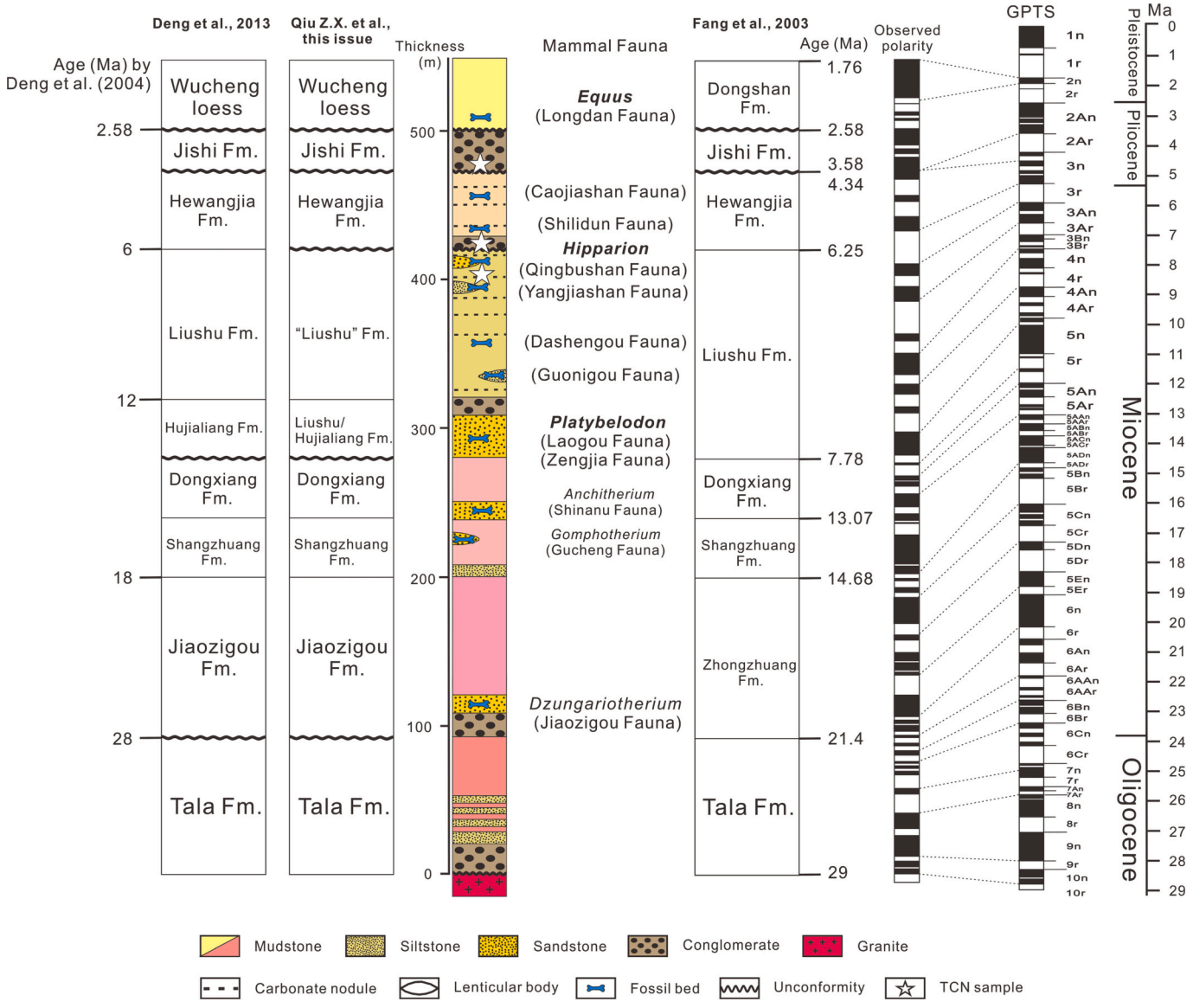

Fig. 2. Composite Cenozoic stratigraphy in the Linxia Basin with mammalian faunas and correlation to GPTS for the magnetostratigraphy of Fang et al. (2003).

sequence and suggested a new stratigraphic division based on mammalian faunas (Fig. 2).

The key to resolving these issues is to obtain the accurate age of the problematic strata. Therefore, paleomagnetic dating has been directly applied to fossil mammal fauna-bearing sediments in recent years. New magnetostratigraphic results show that the *Platybelodon* fauna, the *Hipparion* fauna and the *Equus* fauna lived during 11.1–12.5 Ma, 5.3–11.5 Ma, and 2.2–2.5 Ma in the Linxia Basin, respectively (Zan et al., 2016; Zhang et al., 2019, 2020). These new magnetostratigraphic age constraints are generally in concordance with the biochronology by Deng et al. (2004). Moreover, three sections in the Linxia Basin were paleomagnetically dated, and the magnetostratigraphic correlations indicated that the same formation has inconsistent ages in different sections (Fang et al., 2016). For example, the Liushu Formation in the north Maogou section is constrained to 6–8 Ma, while in the southern piedmont, the Heilinding section has an age range of 6.5–10 Ma. Thus, Fang et al. (2016) used a model to explain the debate on the temporal-spatial variation of stratigraphy and sedimentary facies that may result from a great diachroneity of stratigraphy. A vulnerability that magnetostratigraphy cannot avoid is that fluvial coarse sediments repeatedly appearing in the sedimentary sequence of the Linxia Basin might have potentially affected the accuracy of paleomagnetic age due to various degrees of erosion on the underlying stratum and resulted in erosional hiatuses.

Coarse deposits appearing in the Linxia Basin sedimentary sequence are believed to exert a profound influence on the complete sequence and lead to ambiguity of magnetostratigraphic results. Therefore, the current biomagnetostratigraphy-based chronology of the Linxia Basin lacks absolute age constraints. Coarse deposits are detrimental in magnetostratigraphy, but they are a preferable material for cosmogenic nuclide dating. This radiometric dating technology is a reliable standard method for dating geomorphic features and measuring process rates over 10^2–10^6 year time scales. In view of the importance of site and stratigraphy, an attempt is made to date samples from three late Neogene formations in the eastern Linxia Basin, namely, the late Miocene "Liushu" Formation, the early Pliocene Hewangjia Formation, and the late Pliocene Jishi Formation, by cosmogenic $^{26}Al/^{10}Be$ and $^{10}Be/^{21}Ne$ burial dating. We provide independent radiometric age constraints for these formations and assess the radiometric ages of these three formations for insights into related regional tectonics and associated mammalian faunas.

2. Geological setting

The Linxia Basin is located on the triple junction of the NE Tibetan Plateau, the West Qinling Shan, and the Loess Plateau (Fig. 1A). Laji Shan, Maxian Shan, and West Qinling Shan lie on the west, north, and south edges of the basin, respectively (Fig. 1B). The altitude of the surrounding mountains ranges from 3000 m to 4000 m, and the height of the basin is approximately 1800–2600 m. The Yellow River and its two tributaries, the Daxia River and the Tao River, drain through the basin and deeply incise approximately 500 m during the Quaternary.

The Linxia Basin is a compressional flexural foreland basin, mainly bordered by the WE-trending northwestern Qinling fault to the south and the NS-trending Leiji Shan fault to the west (Fig. 1B). Cenozoic terrestrial sediments unconformably overlie the Caledonian granite rocks at the basin center and the Cretaceous sedimentary rocks in the north. Thick eolian and fluvio-lacustrine sediments were deposited nearly continuously from the Oligocene to Pleistocene in most areas. The Paleogene and Neogene strata are dominated by red siltstone, mudstone, and sandstone, which were deposited in lacustrine and fluvial environments with a maximum thickness of up to 1600 m. Afterward, Quaternary lacustrine sediments and eolian loess with thicknesses of 100–400 m have unconformably overlain on the prior strata (Fang et al., 1997).

As mentioned above, there are two kinds of stratigraphic divisions in the Linxia Basin according to Fang et al. (2003) and Deng et al. (2013a). We will follow a refined biochronologically calibrated division by Deng et al. (2013a) with modest adjustments in nomenclature by Qiu Z.X. et al. (this issue) in this study (Fig. 2). The Cenozoic succession is divisible into eight formations in terms of different sedimentary facies, paleontology, and magnetostratigraphy. In ascending order, they are the early Oligocene Tala Formation, the late Oligocene Jiaozigou Formation, the late Oligocene-early Miocene Shangzhuang Formation, the early-middle Miocene Dongxiang Formation, the middle-late Miocene Liushu/Hujialiang Formation, the late Miocene "Liushu" Formation, the Pliocene Hewangjia Formation, and the early Pleistocene Jishi Formation (Fig. 2). The succession from the Tala Formation to the Hewangjia Formation is characterized by seven cycles (formations) of fining-upward red to yellow siltstone and mudstone and yellowish-gray pebbly sandstone (Fig. 2). Boulder conglomerate of the Jishi Formation unconformably overlies prior folded strata. The Dongshan Formation in the Dongshanding section of the western Linxia Basin mainly consists of lacustrine deposits (Li et al., 1995), while that in the central Linxia Basin generally consists of an eolian loess-paleosol sequence (Deng et al., 2004).

3. Samples and methods

3.1. Sampling sites

The "Liushu" Formation is mainly composed of yellowish-brown carbonate cemented siltstone intercalated with a few thin beds of mudstone with thicknesses of 17–150 m at the basin center, and nearly 200 m-thick gravel beds interbedded with silts appear in the southern piedmont area (Deng et al., 2004). The "Liushu" Formation bears abundant mammalian fossils and contains four *Hipparion* faunal assemblages belonging to the late Miocene. From the lower to the upper, they are Guonigou, Dashenggou, Yangjiashan, and Qingbushan faunas (Deng et al., 2004, 2013b). The Hualin section is situated near Hualin Village at the southern margin of the basin (Fig. 1B) and was recently quarried by the construction of a burial site museum in 2017. Approximately 50 m of braided river deposits are quarried at ~2350 m a.s.l. (Fig. 3A). The gravels are well-rounded, with diameters from 1 cm to 10 cm, and their lithologies include granite, quartzite and mudstone. An amalgamated granite pebble sample (sample LSP) was collected at the bottom of this section at a depth of >30 m (Table 1).

The Hewangjia Formation consists of a ~ 10 m-thick gravel bed at the bottom and ~ 50 m-thick red clay at the upper in the named place (Hewangjia Village at the western margin of the basin). The Caojiashan section in the northern Hezheng City is well exposed by quarry (Fig. 1B). Clastic sediments include a 10 m-thick layer of matrix-supported gravels overlain by 5 m of red silt (Fig. 3B). Quaternary eolian loess overlies the Hewangjia Fm. with a thickness of ~10 m. Gravels are 1–10 cm in diameter and well rounded, and the lithology of pebbles contains quartzite, mudstone, siltstone and limestone. One sand sample (sample HWJS) was collected at the bottom of the gravel bed (Table 1).

The Jishi Formation is also known as the Jishi conglomerate and is dominated by carbonate-cemented well-rounded cobbles (Fig. 3C). No fossils have been found in this formation (Deng et al., 2004). The thickness of the Jishi Formation varies greatly in the basin and could reach a maximum thickness of 60 m near the Jishi Shan, which is the named site on the western margin of the basin. Normal thickness of the Jishi Formation ranges from 10 m to 30 m at the basin center. In Youhao Village, ~1 km east of the Caojiashan section (Fig. 1B), the Jishi Formation has a thickness of ~20 m, unconformably overlies the Hewangjia Formation, and is covered by approximately 5 m eolian loess. Yellow carbonate cemented well-rounded pebbles and cobbles (up to 20 cm in size) with massive bedding or roughly imbricated structures and many intercalated lenses of sandstone can be observed in this section (Fig. 3C). One sand sample (sample JSS) was collected in an interbedded sandy lens at the bottom of conglomerates (Table 1).

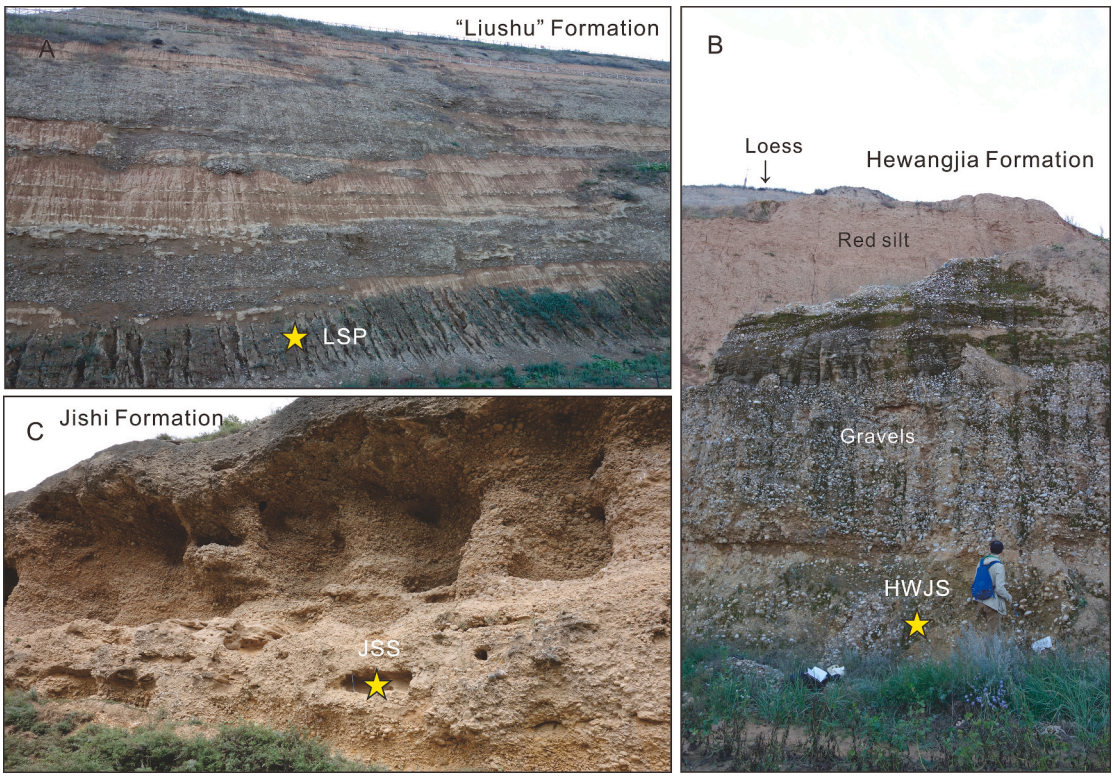

Fig. 3. Field pictures of the sampled formations (yellow star indicates sampling position). (A) A new quarried section of the upper "Liushu" Formation with a 50 m thickness of braided river deposition next to the Hualin burial site museum. (B) A new quarried section of the Hewangjia Formation at the Caojiashan section, showing a gravel bed of river channel and siltstone and mudstone of overbank floodplain above and capped by eolian loess. (C) A new quarried section of the Jishi Formation, showing a carbonate cemented conglomerate bed with a total thickness of 20 m in Youhao Village. (For interpretation of the references to colour in this figure legend, the reader is referred to the web version of this article.)

Table 1
Sample information.

Sample name	Formation	Latitude (°N)	Longitude (°E)	Altitude (m a.s.l.)	Sample type	Present sample depth (m)
JSS	Jishi	35.4770	103.3643	2378 ± 3	Sand	20
HWJS	Hewangjia	35.4743	103.3535	2363 ± 2	Sand	22
LSP	"Liushu"	35.3626	103.4175	2349 ± 3	Pebbles	≥ 30

3.2. Burial dating with $^{26}Al/^{10}Be$

Cosmogenic nuclide burial dating uses measurements of the concentrations of ^{10}Be and ^{26}Al in samples that were exposed to Earth's surface before deposition and shielding from cosmic rays. Once buried, the ^{26}Al and ^{10}Be contents decrease due to radioactive decay, and the faster decay of the relatively short-lived ^{26}Al results in a decrease in ^{26}Al/^{10}Be. The ^{26}Al/^{10}Be ratio is used to derive a burial age assuming closed system behavior (Granger and Muzikar, 2001; Granger, 2006; Granger, 2014).

The long-term concentration (N_i) of ^{26}Al or ^{10}Be in quartz that is exposed near the surface and then buried follows the relationship:

$$N_i = N_{i,inh}e^{(-t/\tau_i)} + N_{i,pb} \quad (1)$$

where subscript i represents either ^{26}Al or ^{10}Be, *inh* indicates inheritance prior to burial (atoms/g), t is burial age (yr), τ is the radioactive mean life (yr) and *pb* indicates the total post-burial production (atoms/g). In a landscape that is eroding steadily at a rate E (m/Ma), the inherited nuclide concentration is:

$$N_{i,inh} = P_n/(1/\tau_i + \rho E/\Lambda_n) + P_\mu/(1/\tau_i + \rho E/\Lambda_\mu) \quad (2)$$

where P_n, P_μ and Λ_n, Λ_μ are the production rates (atoms/g/yr) and penetration lengths (g/cm^2) due to neutrons and muons, respectively, and ρ indicates rock density (g/cm^3). Simple burial dating assumes that the sample accumulated ^{26}Al and ^{10}Be during exhumation and transport and was then buried deeply enough (typically >10 m) that post-burial production can safely be ignored. In this case, Eq. (1) simplifies to

$$N_{26}/N_{10} = (N_{26,inh}/N_{10,inh})e^{-t(1/\tau_{26}-1/\tau_{10})} \quad (3)$$

Eq. (2) and Eq. (3) can be solved iteratively for the converging solution of burial age t and pre-burial erosion rate E.

The basic premise of burial dating is that sediment is buried deep enough to avoid significant post-burial nuclide production and has not been previously buried. Thus, burial dating is ideal for dating cave sediments or very thick fluvial deposits. The current burial dating method limits range roughly between 0.1 and 5 Ma (Granger, 2014).

The paleo-elevation estimation of the study area for local cosmogenic nuclide production rate calculation is difficult. There are two topographic estimates based on different paleo-altimetry proxies at present. Pieces of evidence based on the paleo-karst landscape, *Hipprion* fauna distribution, and pollen assemblages suggest that a widespread planation surface developed on the plateau until the Pliocene and that the elevation was <1000 m (Li et al., 1979, 1995). But new palynological records and magnetostratigraphy from the neighboring Xining Basin and Lanzhou Basin suggest that this part of the northeastern Tibetan Plateau

has been at a high elevation (>3000 m) since at least ~38 Ma (Dupont-Nivet et al., 2008; Hoorn et al., 2012; Miao et al., 2013). However, paleo-elevation affects the production rate of ^{10}Be and ^{26}Al, but their ratio (~6.8) that correlates with burial age calculation is generally independent of elevation. Therefore, $P_{n\&\mu,10}$ = 30.9 atoms/(g·a) and $P_{n\&\mu,26}$ = 208.8 atoms/(g·a) were calculated for an average upper drainage basin elevation of 3000 m by the Lal/Stone model (Lal, 1991; Stone, 2000) using the CRONUS-earth online calculator v.2.3 MATLAB code. Local cosmogenic nuclide production rates in the study area were assumed to be constant for the basin. The regression was performed based on York et al. (2004).

3.3. Burial dating with ^{21}Ne/^{10}Be

The combination of stable cosmogenic nuclide ^{21}Ne, which is also produced in quartz, with ^{10}Be allows us to date buried materials up to 15 Ma (Balco and Shuster, 2009). However, the presence of non-cosmogenic neon components in minerals adds uncertainty to the accuracy of age determined by cosmogenic ^{21}Ne. Thus, only a few studies have employed ^{21}Ne/^{10}Be burial dating (e.g., Balco and Shuster, 2009; Ma et al., 2018). If taking no account of the post-burial nuclide concentrations, a ^{21}Ne/^{10}Be burial age can be calculated based on Eq. (1):

$$t_b = -\left(\frac{1}{\lambda_{10}}\right)\cdot ln\left[\left(\frac{N_{10}}{N_{21}}\right)\cdot\left(\frac{P_{21}}{P_{10}}\right)+\left(\frac{N_{10}}{P_{10}}\right)\cdot\lambda_{10}\right] \quad (4)$$

where λ_{10} is the radioactive decay constant of ^{10}Be, which is the inverse of mean life ($\lambda = 1/\tau$), and we used a value of (4.987 ± 0.043) × 10^{-7} per year (Chmeleff et al., 2010). P_{21}/P_{10} is the production ratio of 4.23 defined in Kober et al. (2011).

3.4. Sample preparation and analysis

Quartz was separated and purified in the State Key Laboratory of Environmental Geochemistry, Institute of Geochemistry, Chinese Academy of Sciences. Beryllium and aluminum extraction and purification, accelerator mass spectrometry (NEC 5MV AMS) measurement of ^{26}Al and ^{10}Be concentration, and total Al determination by inductively coupled plasma optical emission spectrometer (ICP − OES, PerkinElmer, Optima 5300DV, assigned 3% uncertainty) were all performed at the Scottish Universities Environmental Research Centre (SUERC). The 0.125–0.25 mm size fraction was used for quartz purification by selective chemical dissolution (Kohl and Nishiizumi, 1992). The purified quartz (20–25 g) was dissolved in a solution of concentrated HF and HNO_3. Approximately 0.2 mg Be carrier was added to the samples and blank. Al carrier (1.0 mg) was added only to the blank. Al and Be were extracted and separated by ion chromatography and selectively precipitated as hydroxides. The precipitates were oxidized at 800 °C. Al_2O_3 and BeO were mixed with Ag and Nb matrices, respectively, with weight ratios of Al_2O_3:Ag = 1:2 and BeO:Nb = 1:6 for AMS analysis (Xu et al., 2015). The measured ^{26}Al/^{27}Al and ^{10}Be/^{9}Be ratios were normalized to primary standards Z92–0222 with a nominal ^{26}Al/^{27}Al ratio of 4.11 × 10^{-11} and NIST SRM 4325 with a nominal ^{10}Be/^{9}Be ratio of 2.79 × 10^{-11}. The procedural blank processed in association with the samples has a ^{10}Be/^{9}Be ratio of (3.04 ± 0.49) × 10^{-15} and ^{26}Al/^{27}Al ratio of (1.94 ± 0.79) × 10^{-15}.

Neon analysis was carried out in the State Key Laboratory of Earthquake Dynamics, Institute of Geology, China Earthquake Administration. Neon extraction was performed under one-step heating at 1350 °C on a noble gas mass spectrometer (model GV 5400). Excess ^{21}Ne was calculated by assuming two components mixing atmospheric and cosmogenic neon, and no neon blank correction was made to the data. For all samples and calibrations, the abundances of masses 2, 16, 18, 19, 20, 21, 22, 40, and 44 were determined. Corrections for $^{40}Ar^{2+}$ at mass 20 and $^{44}CO_2^{2+}$ at mass 22 were calculated from the measured mass 40 ($^{40}Ar^{+}$) and mass 44 ($^{44}CO_2^{2+}$) signals by using their individual charge state ratios of $^{40}Ar^{+}/^{40}Ar^{2+}$ = 4.18–4.20 and $^{44}CO_2^{+}/^{44}CO_2^{2+}$ = 104–106. The isobaric interference from $H_2^{18}O^{+}$ and $H^{19}F^{+}$ at mass 20 can be ignored. Detailed information about the measurement procedure can be found elsewhere (Codilean et al., 2008; Ma et al., 2015). CREU quartz (Vermeesch et al., 2015) was used as an internal standard.

4. Results

All analytical results are listed in Table 2–3 and Fig. 4. The stated errors are 1σ calculated from AMS and ICP–OES uncertainties.

A ^{26}Al/^{10}Be burial age of 2.50 (+0.20/−0.18) Ma was determined for the bottom sand sample of the Jishi Formation (Table 2; Fig. 4A). The lower gravel bed of the Hewangjia Formation yields a ^{26}Al/^{10}Be burial age of 3.06 (+0.36/−0.31) Ma (Table 2; Fig. 4A). The ^{10}Be/^{9}Be ratio of the "Liushu" Formation is as low as (2.01 ± 0.10) × 10^{-14} and only an order of magnitude higher than the blank level, leading to a higher uncertainty of the ^{10}Be concentration.

For the neon measurement, the isotope ratio lies on the spallation line within the uncertainty in the neon three-isotope diagram illustrated in Fig. 4B, indicating no significant non-cosmogenic ^{21}Ne released before 1350 °C. The resultant cosmogenic ^{21}Ne concentration of sample LSP is (1.49 ± 0.07) × 10^{7} atoms/g, leading to a ^{10}Be/^{21}Ne burial age of 11.70 ± 0.17 Ma (Table 3; Fig. 4C). The non-atmospheric ^{21}Ne in the sample includes unresolved contributions of nucleogenic Ne, therefore the burial age of 11.70 Ma represents the maximum age when assuming a simple exposure−burial history. Post-burial nuclide production involving spallation and muon reactions was not considered in this study given a minor contribution to the total nuclide concentration (Ma et al., 2018).

5. Discussions

5.1. Age interpretation of the three studied formations

For the cosmogenic nuclide simple burial age, the assumptions of (1) no inherited nuclide concentrations and (2) no post-burial nuclide production would have opposite effects on the burial age calculation, N_{inh}-induced overestimation, and N_{post}-induced underestimation for the sample's burial age. On the basis of the different circumstances of individual samples, we would interpret differently on each age.

5.1.1. Jishi Formation

In conventional cases, N_{inh} in the source rocks is negligible for radionuclides. Nevertheless, in our study, the source of the Jishi Formation is probably the late Neogene sediments, in which the radionuclides still have high concentrations and cannot be neglected. Therefore, the ^{26}Al/^{10}Be burial age of 2.50 (+0.20/−0.18) Ma of the Jishi Formation may have been overestimated based on the following geological evidence. The "Liushu" Formation only left 17 m and was capped by the Jishi Formation in the Laogou section (basin center), where the upper part of the "Liushu" Formation and the whole Hewangjia Formation were completely eroded (Deng et al., 2004). Our sampling site of the Jishi Formation is located at the basin center (Fig. 1B), therefore we suppose that the old deposits from these two formations were most probably eroded and carried into the deposition of the Jishi Formation. The inherited low ^{26}Al/^{10}Be ratio may have decreased the sediment pre-burial ^{26}Al/^{10}Be ratio, making deposits appear older.

Owing to the absence of vertebrate fossils and coarse-grained deposits, the timing of the Jishi Formation depends largely on biochronology and magnetostratigraphy from overlying and underlying strata. Although paleomagnetic data points were obtained from the same lithological unit at the Wangjiashan section in the western Linxia Basin (Li et al., 1997; Fang et al., 1997, 2003), the reliability of the signals retrieved from the conglomerates has never been elaborated in previous studies. In consideration of the overlying loess-paleosol and lacustrine sequences yielding Quaternary *Equus* fauna, as well as the

Table 2
Cosmogenic nuclide ^{26}Al and ^{10}Be data of the dated samples.

Sample	Quartz mass (g)	Al (ppm)	$^{27}Al/^{26}Al$ (10^{-14})	$^{10}Be/^{9}Be$ (10^{-14})	Concentration (atoms/g)		$^{26}Al/^{10}Be$	Burial age (Ma)
					^{26}Al (10^4)	^{10}Be (10^4)		
JSS	22.09	139 ± 2	2.26 ± 0.19	5.44 ± 0.17	7.02 ± 0.59	3.44 ± 0.13	2.04 ± 0.19	2.50 (+0.20/−0.18)
HWJS	20.91	213 ± 2	0.90 ± 0.14	4.35 ± 0.16	4.26 ± 0.66	2.74 ± 0.13	1.56 ± 0.25	3.06 (+0.36/−0.31)
LSP	25.89	79 ± 1		2.01 ± 0.10		0.10 ± 0.07		

Table 3
Neon isotope data of the sample LSP from the "Liushu" Formation.

Sample	Weight (g)	T(°C)	Concentration (atoms/g)		$^{21}Ne/^{20}Ne$ (10^{-3})	$^{22}Ne/^{20}Ne$ (10^{-3})	$^{21}Ne_{cos}$ (10^7 atoms/g)	^{10}Be-^{21}Ne age (Ma)
			^{20}Ne (10^9)	^{21}Ne (10^7)				
LSP	0.41	1350	17.56 ± 0.05	6.50 ± 0.23	3.81 ± 0.14	103.03 ± 1.00	1.49 ± 0.07	11.70 ± 0.17

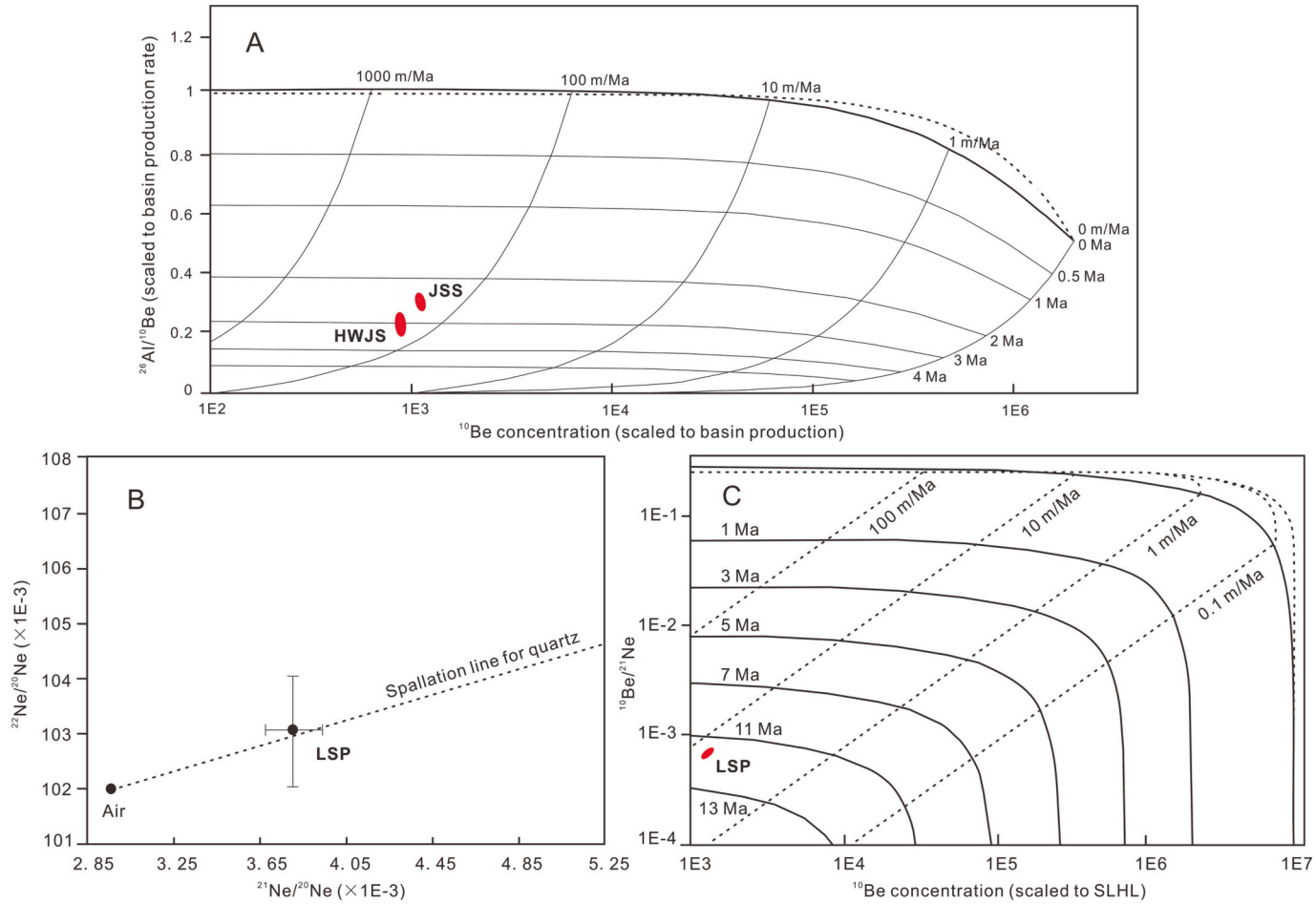

Fig. 4. (A) Cosmogenic nuclide data of the Jishi Formation and Hewangjia Formation, shown on a $^{26}Al/^{10}Be$ exposure-burial diagram. Labeling of sample acronyms as used in Table 1. (B) Ne three isotope diagram for the upper "Liushu" Formation sample showing the Ne isotope ratios of the component. (C) $^{21}Ne/^{10}Be$ exposure-burial diagram of sample LSP.

underlying Hewangjia Formation bearing Shilidun local fauna of early Pliocene (Deng et al., 2004, 2013a, 2013b), the Jishi Formation was generally regarded as a late Pliocene sequence (Li et al., 1997; Fang et al., 1997, 2003; Deng et al., 2004, 2013a, 2013b).

Based on this assumption, different magnetostratigraphic studies of the overlying Quaternary successions provided similar age constraints to the early Pleistocene *Equus* fauna therein (Li et al., 1997; Liu et al., 2008; Zan et al., 2016). Li et al. (1997) reported the magnetostratigraphy from two long Quaternary sequences in the western Linxia Basin, which are composed of eolian loess-paleosol in the upper part and lacustrine silts in the lower part. A prolonged normal magnetozone (N6) obtained from the lower part of the Dongshanding section was correlated to the Olduvai normal subchron (Fig. 5A), meanwhile, the *Equus* fossils from the Wangjiashan section, which shared a similar polarity pattern to that of the Dongshanding sequence, were considered to yield from the reversed polarity (R6) just below this long normal one (Li et al., 1997). Liu et al. (2008) presented a short magnetostratigraphic sequence from an outcrop near the fossil sites of the Longdan local fauna, while Zan et al.

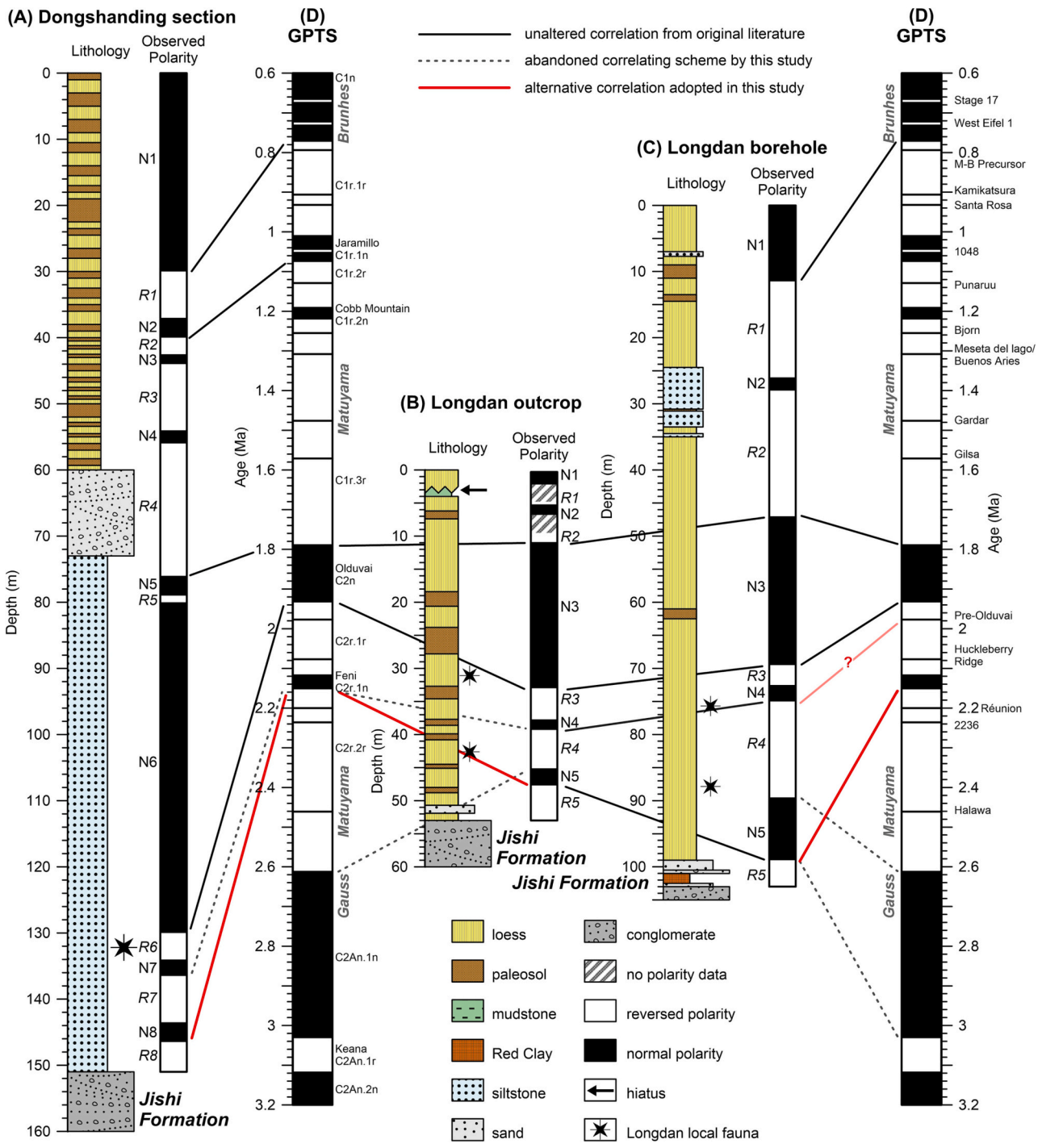

Fig. 5. Previous lithostratigraphic and magnetostratigraphic studies of (A) the Dongshanding section (modified from Li et al., 1997), (B) the Longdan outcrop (modified from Liu et al., 2008), and (C) the Longdan borehole (modified from Zan et al., 2016), and their correlation to (D) the GPTS (Geomagnetic Polarity Time Scale, Singer, 2014; Singer et al., 2014; Ogg, 2020) by different studies.

(2016) exhibited another one from a long borehole succession in the same area. The latter two studies demonstrated a similar prolonged normal magnetozone overlying two short normal ones in the lower part of the sequence (Fig. 5B and C). The authors all correlated the lowermost normal magnetozone (N5 in Fig. 5B and C) to subchron C2An.1n of the Gauss Chron spontaneously based on the assumption that the Jishi Formation was assigned to the late Pliocene (Liu et al., 2008; Zan et al., 2016). The age range of the Longdan *Equus* fauna, thus, was constrained within a long time span from Chrons C2r.2r to C2n (from early Matuyama Chron to early Olduvai subchron).

Our first radiometric age by the $^{26}Al/^{10}Be$ burial dating technique of the Jishi Formation suggests that its initial deposition age in this site was no earlier than 2.50 (+0.20/−0.18) Ma. This absolute dating of the conglomerate layers provides us with new insight into the timing of the fauna from the younger strata (Fig. 5). The sequences above the Jishi Formation, including the eolian loess/paleosol and lacustrine silts, may have been deposited during the Chinese Nihewanian Stage/Age of Quaternary (Deng et al., 2019a; Sun et al., 2021). Consequently, the correlations between N5 in the lower part of the two Longdan sequences and subchron C2An.1n (Fig. 5B and C) are problematic. With the new

absolute age of the Jishi Fm. in this study, we are able to recalibrate the lower part of the previous age models of the Quaternary lithostratigraphy of the Linxia Basin. The consistent magnetozones N5 from the basal Longdan outcrop and borehole and N8 from the bottom of the Dongshanding section are preferred to reassign to Feni (formerly Réunion, see Singer, 2014) normal subchron instead of C2An.1n of late Gauss Chron (Fig. 5A–C). Another isolated interval of normal polarity above it was identified from all three sequences (N7 in Fig. 5A, N4 in Fig. 5B and C). Whether this magnetozone could be accurately associated with certain short-lived geomagnetic excursions between Olduvai and Feni subchrons (i.e., pre-Olduvai at 1.977 Ma and Huckleberry Ridge at 2.077 Ma, Singer et al., 2014, Fig. 5D) needs further verification. Our recalibrated age model, which is similar to the original interpretation of Fang et al. (1997) in some ways, also acknowledges the paradoxical conclusion on a loess/paleosol sequence with a basal age at the beginning of Chron C2An.1n (3.032 Ma; Ogg, 2020) (Yang and Ding, 2010). Therefore, the ages of the upper and lower Longdan *Equus* fauna are now constrained between subchrons C2r.1r and early C2n with a narrower temporal interval of ca. 2.1–1.9 Ma.

Although shared with a few fossil mammal components, the Longdan local fauna is supposed to be slightly earlier than the classic Nihewan fauna (sensu stricto, i.e., the Xiashagou local fauna) in the Nihewan Basin in northern China (Qiu et al., 2004b). The Xiashagou local fauna persisted from ca. 2.2 Ma to ca. 1.7 Ma based on magnetostratigraphic dating (Liu et al., 2012), which has been independently supported by the $^{26}Al/^{10}Be$ isochron burial dating to 2.05 ± 0.38 (0.39) Ma recently (Tu et al., 2022). The first appearance of the lower fossiliferous layer of the Longdan local fauna at ca. 2.1 Ma is consistent with these biochronological estimations.

5.1.2. *Hewangjia Formation*

The $^{26}Al/^{10}Be$ burial age of 3.06 (+0.36/−0.31) Ma places the lower clast sedimentation of the Hewangjia Formation in the eastern Linxia Basin to the late Pliocene. Unlike in the Jishi Formation, there is no obvious geological evidence suggesting significant $^{26}Al/^{10}Be$ pre-burial inheritance. Therefore, in consideration of the post-burial muon production possibility, the age of 3.06 Ma may be interpreted as an underestimated age for the lower Hewangjia Formation. This age is significantly younger than the previous paleomagnetic age of 6.16–6.25 Ma in the same gravel layer in the Wangjiashan section of the western Linxia Basin indicated by Li et al. (1995) and Fang et al. (1997, 2003). The radiometric $^{26}Al/^{10}Be$ ages of the Jishi Formation and the lower Hewangjia Formation imply that the accumulation of the red clay of the upper Hewangjia Formation at our sampling site persisted to the late Pliocene. This result is inconsistent with the previous palaeomagnetic age of 4.3–6.2 Ma in the Wangjiashan section (Li et al., 1995; Fang et al., 1997) and conflicts with the latest magnetostratigraphic study indicating that the *Hipparion* fauna fossils found in the upper Hewangjia Formation were at ~5.3 Ma in the Duikang section, which is ~20 km east of our sampling site (Zhang et al., 2019). The *Hipparion* fauna found in red clays 3 m above the basal gravels of the Hewangjia Formation in the Shilidun section, close to the Duikang section, was assigned to the Shilidun fauna by Deng et al. (2013a) and inferred to the early Pliocene, which corresponds to the Gaozhuangian Stage/Age of biochronology in China and MN 14 of the European mammal zones (Deng et al., 2004, 2019b).

However, new micro-mammalian fossils found in the red clay of the upper Hewangjia Formation at the same sampling site, which are named Caojiashan fauna, suggest that the strata are from the late Pliocene, roughly equivalent to MN 16 of the European land mammal zonation (Qiu Z.D. et al., this issue). This latest biochronological estimation strongly supports our radiometric age, and these two methods could independently constrain the age of the Hewangjia Formation at this site. The age estimation difference of the Hewangjia Formation between different sections, as mentioned above, could be preliminarily explained by the diachroneity of stratigraphy or its distinct preservation at different localities. Hence, our radiometric age that was directly dated on the gravel bed would be reliable and postpone the Hewangjia Formation in the Caojiashan section into the late Pliocene. The Hewangjia Formation is now verified to persist until the late Pliocene in the eastern Linxia Basin.

5.1.3. *"Liushu" Formation*

The sampling site of the upper "Liushu" Formation near Hualin Village yields a $^{10}Be/^{21}Ne$ age of 11.70 ± 0.17 Ma. Our sampling section lies exactly on the fossiliferous bed of the Yangjiashan fauna of the *Hipparion* fauna in the burial site museum of Hualin (personal communication with T. Deng). This kind of *Hipparion* fauna was speculated to be from the late Miocene and could correlate with the late Bahean Stage/Age of biochronology in China and MN 11/12 of the European mammal zones (Deng et al., 2013b, 2019b). The lower boundary of the Bahean Stage/Age was expediently assigned to 11.63 Ma within chron. C5r.2n of the geomagnetic polarity timescale (GPTS) (Fang et al., 2016; Deng et al., 2019b), which is characterized by the appearance of the oldest Chinese *Hipparion* fauna that was also known as the Guonigou fauna (Deng et al., 2013b, 2019b). This lowermost level of *Hipparion* fauna produced in the lower Liushu Formation could correspond with the Tortonian stage and MN 9 of the European mammal zones (Qiu and Qiu, 1995; Qiu et al., 1999; Deng et al., 2013b, 2019b). The boundary of the Bahean/Baode Stage was expediently correlated to the beginning of the Messinian stage since 7.25 Ma (Hilgen et al., 2000; Deng et al., 2013b, 2019b). Nevertheless, a new study of an early Baodean assemblage from Inner Mongolia inferred that this boundary may be earlier than 7.64 Ma (Sun et al., 2018), indicating that the age of the Yangjiashan fauna should be older than 7.64 Ma. Recent paleomagnetic dating of the Yangjiashan fauna agrees with this view and suggests that its age is ~8.2 Ma (Zhang et al., 2019). However, the typical elements in the Dashengou fauna such as *Dinocrocuta gigantea* and *Hezhengia bohlini*, disappeared in the Yangjiashan fauna, and Yangjiashan fauna is similar to but slightly older than the Baodean fauna (Deng et al., 2013b, 2019b). Consequently, we suggest that the age of the Yangjiashan fauna should range between 7.6 Ma and 8.2 Ma.

The youngest *Hipparion* fauna found in the top "Liushu" Formation was named Qinbushan fauna and ascribed to the Baodean Stage by Deng et al. (2013b, 2019b). The Qinbushan fauna was estimated to be approximate ~6.3 Ma at different sections in the Linxia Basin (Li et al., 1995; Fang et al., 1997, 2003, 2016; Zhang et al., 2019). Therefore, our sample LSP collected above the Yangjiashan fauna and beneath the Qinbushan fauna should yield an age of 6.3–8.2 Ma according to the bio-magnetostratigraphic studies mentioned above. However, the $^{10}Be/^{21}Ne$ age of 11.70 ± 0.17 Ma obtained in this study is only on the lower boundary of the Bahean Stage/Age, indicating that the deposition age of the upper "Liushu" Formation should be younger than 11.7 Ma attributed to the unsolved non-cosmogenic ^{21}Ne concentration. This age is older than previous bio-magnetostratigraphic work but generally agrees with the new bio-magnetostratigraphic framework of "Liushu" Formation (Qiu Z.X. et al., this issue; Zheng et al., 2023; Sun et al., 2023).

It is important to note that the cosmogenic burial age estimations of the three samples from three lithological units in this study might only represent the sedimentation age of the formation of individual sites. However, the present results have shown the potential application of cosmogenic nuclide dating in the Linxia Basin. In future work, more cosmogenic nuclide dating technique (especially isochron burial dating) combined with the bio-magnetostratigraphic method would not only provide accurate constraints to the chronostratigraphic framework but also help conclude the debate about the diachroneity of stratigraphy in the Linxia Basin.

5.2. *Regional geological implications*

An abrupt change in lithology in the Linxia Basin occurred at 2.5 Ma, marked by a change from the alternations of lacustrine-based and short

intervals of fluvial deposition before 2.5 Ma to the very uniform gravel deposits of the Jishi Formation. This kind of angular unconformity conglomeratic sedimentation widely occurs in the different margins of the Tibetan Plateau and makes it the most striking marker strata for stratigraphic correlation in western China. For instance, there are the Xiyu conglomerates along the Tian Shan, Kunlun Shan, and Altun Shan, the Yumen conglomerates along the Qilian Shan, and the Dayi conglomerates in front of the Longmen Shan (Fig. 6). In addition, these thick molasse deposits were synchronously deposited at ~3.6 Ma, as inferred by earlier magnetostratigraphy and electron spin resonance dating (Li, 1991; Fang et al., 2004; Li et al., 2006). Therefore, Li et al. (1996) attributed the origin of these conglomerates to intensive tectonic movement and named them the first episode of the Qing-Zang Movement (QZM A, ~3.6 Ma), which is normally regarded as the initial accelerated uplift of the Tibetan Plateau in the late Cenozoic. However, Zheng et al. (2006) queried this interpretation of the Jishi conglomerates and attributed them to the local uplift of the Jishi Shan instead. Based on the apatite fission track data, the Jishi Shan was uplifted high enough (200–900 m) to result in relief precipitation and traverse river origination. Then, coarse sediments were discharged from the Jishi Shan and deposited in the basin by these rivers. Thus, the Jishi conglomerates were argued to be unqualified as a proxy for the onset deformation and uplift of the Tibetan Plateau (Zheng et al., 2006a, 2006b).

An alternative view is that the piedmont conglomerate involving the Jishi conglomerates was a product of climate change. Some studies have proposed that these large-grained sediments deposited 2–4 Ma ago were primarily caused by the increased erosion rates as a result of global climate change (e.g. Molnar and England, 1990; Zhang et al., 2001). Kong et al. (2011) used the glacial activity before 2 Ma to interpret the deposition of the Dayi conglomerates in eastern Tibet. Stable carbon and oxygen isotope analyses of the Xiyu conglomerates from the northern margin of the Tian Shan indicate that climate change has a non-negligible effect on the occurrence of these coarse deposits (Deng et al., 2008). Sun et al. (2004) also suggested that the accumulation of the early Pleistocene Xiyu conglomerates in the same study area was controlled by both tectonics and climatic cooling. By contrast, the sedimentation rate of the Yumen conglomerates in front of the Qilian Shan increases northwestwardly, which is coincident with the present-day topography rather than the annual precipitation (Liu et al., 2011). This research suggested that the deposition of conglomerates was mainly in response to tectonic uplift.

In recent years, a large number of chronologic works have demonstrated that these thick conglomerates were asynchronously deposited at different mountain rims. Magnetostratigraphic studies show that the basal age of the Xiyu conglomerates is diachronous and can range from the Miocene to the Quaternary (~15–1 Ma) in different regions (e.g. Sun et al., 2004; Charreau et al., 2009; Heermance et al., 2007). Our results, together with previous cosmogenic dating studies suggest that the Yumen, Jishi, and Dayi conglomerates were deposited at ~5 Ma (Zhao et al., 2017), 2.5 Ma (this study), and 2.0 Ma (Kong et al., 2011), respectively. As mentioned above, the deposition of conglomerates around Tibet, including the Siwalik Group (upper Siwalik) in the Himalayan foreland basin, was asynchronous and had multiple causes along the different orogens rather than a particular tectonic and/or climate event, as previously thought.

Nevertheless, a strong tectonic movement indeed occurred in the

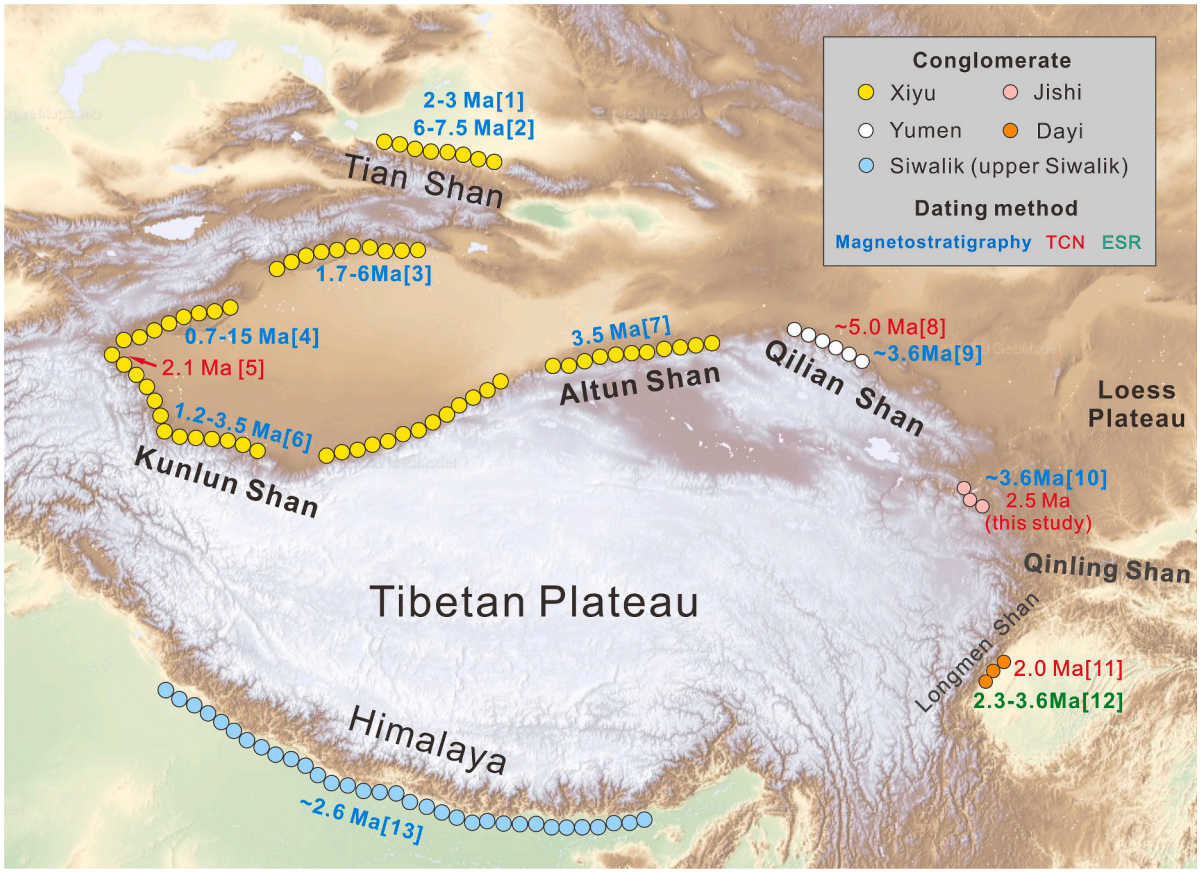

Fig. 6. The distribution of some conglomerates around the Tibetan Plateau. Reference codes are as follows: [1] = Sun et al. (2004, 2007), Li et al. (2011), Sun and Zhang (2009); [2] = Ji et al. (2008, 2010) and Charreau et al. (2009); [3] = Sun et al. (2009), Huang et al. (2010), Jing et al. (2011) and Zhang et al. (2014); [4] = Chen et al. (2007), Heermance et al. (2007) and Qiao et al. (2017); [5] = Han et al. (2015); [6] = Zheng et al. (2006a, 2006b) and Sun and Liu (2006); [7] = Ma (2007); [8] = Zhao et al. (2017); [9] = Fang et al. (2004); [10] = Li et al. (1995), Fang et al. (1997, 2003); [11] = Kong et al. (2011); [12] = Li et al. (2006) and Wang et al. (2003); [13] = Nakayama and Ulak (1999), Sinha et al. (2007) and Chirouze et al. (2012).

Linxia Basin, as mentioned above, that is, the upper part of the "Liushu" Formation and the whole Hewangjia Formation were completely eroded (Deng et al., 2004). The tectonics had significant effects on the accumulation of the Jishi Formation. The role of climate change in the Linxia Basin has not been adequately addressed over the timespan of interest. However, the onset of large ice sheets in the high northern latitudes has been firmly documented around ~2.6 Ma, followed by a series of glacial and interglacial cycles. Climate change most likely affects conglomerate production through the control of glacial erosion in the high mountains. The intricate controls of tectonics and climate change over time and their signatures are often mixed and difficult to resolve. Therefore, we see tectonic uplift was the dominant driving force for the accumulation of Jishi conglomerates in the Linxia Basin and that climate cooling might have played a minor role in this process.

6. Conclusions

The cosmogenic $^{26}Al/^{10}Be$ and $^{10}Be/^{21}Ne$ burial dating applied on the upper "Liushu" Formation, lower Hewangjia Formation, and lower Jishi Formation in the Linxia Basin provides reliable age constraints for its chronostratigraphy. The upper "Liushu" Formation yields a cosmogenic $^{10}Be/^{21}Ne$ burial age of 11.70 ± 0.17 Ma, in contrast to the findings from previous bio-magnetostratigraphy, this age may have been overestimated due to indistinguishable nucleogenic ^{21}Ne from the total concentration. The underestimated $^{26}Al/^{10}Be$ age of the Hewangjia Formation is 3.06 (+0.36/−0.31) Ma, and the overestimated $^{26}Al/^{10}Be$ age of the Jishi Formation is 2.50 (+0.20/−0.18) Ma, suggesting that the previous bio-magnetostratigraphic ages need correction. The time span of the Longdan *Equus* local faunas yielded from the strata above the Jishi Formation is thus between C2r.1r and early C2n (ca. 2.1–1.9 Ma). Our new data demonstrate that accelerated uplift recorded by the Jishi Formation on the northeastern margin of the Tibetan Plateau occurred from 2.5 Ma to 3.1 Ma ago, which is younger than the previous estimation of ~3.6 Ma. In future work, the $^{26}Al/^{10}Be$ isochron burial dating method could be tried on the Jishi Formation and the Hewangjia Formation, which would help with identifying recycled materials and addressing post-burial production. In addition, for more accurate age constraints on the upper "Liushu" Formation, we will attempt to correct for nucleogenic neon by determining neon isotopes in the deep shielded parent rock from the source areas. If applicable, accurate radiometric ages of the older strata could be obtained from $^{10}Be/^{21}Ne$ burial dating, which will greatly improve the understanding of the chronology of the Linxia Basin.

Declaration of Competing Interest

The authors declared that they have no conflicts of interest to this work.

We declare that we do not have any commercial or associative interest that represents a conflict of interest in connection with the work submitted.

Data availability

Data will be made available on request.

Acknowledgements

We are grateful to Prof. Tao Deng at Key Laboratory of Vertebrate Evolution and Human Origins, Institute of Vertebrate Paleontology and Paleoanthropology, Chinese Academy of Sciences for useful suggestion and discussion. This research was funded by the Strategic Priority Research Program of the Chinese Academy of Sciences (XDB40020300), National Natural Science Foundation of China (41473055 and 41401009), Autonomous Deployment Program of the State Key Laboratory of Environmental Geochemistry (E2KJA10001) and Cooperative Project of Research Institute of Exploration and Development, Sinopec, Northwest Oilfield Company (KY2022-S-028). We thank Drs. Lawrence Flynn, William Odom, and one anonymous reviewer for their constructive comments and suggestions that greatly improved the manuscript.

References

An, Z.S., Kutzbach, J.E., Prell, W.L., Porter, S.C., 2001. Evolution of Asian monsoons and phased uplift of the Himalaya-Tibetan Plateau since late Miocene times. Nature 411, 62–66.

Balco, G., Shuster, D.L., 2009. 26Al-10Be-21Ne burial dating. Earth Planet. Sci. Lett. 286, 570–575.

Charreau, J., Gumiaux, C., Avouac, J.P., Augier, R., Chen, Y., Barrier, L., Gilder, S., Dominguez, S., Charles, N., Wang, Q.C., 2009. The Neogene Xiyu Formation, a diachronous prograding gravel wedge at front of the Tianshan: climatic and tectonic implications. Earth Planet. Sci. Lett. 287, 298–310.

Chen, J., Heermance, R.V., Burbank, D.W., Scharer, K.M., Wang, C.S., 2007. Magnetochronology and its implications of the Xiyu conglomerate in the southwestern Chinese Tian Shan foreland. Quat. Sci. 27, 576–587 (in Chinese with English abstract).

Chirouze, F., Dupont-Nivet, G., Huyghe, P., Beek, P., Chakraborti, T., Bernet, M., Erens, V., 2012. Magnetostratigraphy of the Neogene Siwalik Group in the far eastern Himalaya: Kameng section, Arunachal Pradesh, India. J. Asian Earth Sci. 44, 117–135.

Chmeleff, J., Blanckenburg, F., Kossert, K., Jakob, D., 2010. Determination of the 10Be half-life by multicollector ICP–MS and liquid scintillation counting. Nucl. Inst. Methods Phys. Res. B 268, 192–199.

Codilean, A.T., Bishop, P., Stuart, F.M., Hoey, T.B., Fabel, D., Freeman, S.P.H.T., 2008. Single-grain cosmogenic 21Ne concentrations in fluvial sediments reveal spatially variable erosion rates. Geology 36, 159–162.

Deng, S.T., Wu, C.D., Gu, X., Guo, Z.J., 2008. Sedimentary records and paleoenvironmental significance if stable isotopic evidences from the late Cenozoic, northern Tianshan. Acta Petrol. Sin. 24, 689–698 (in Chinese with English abstract).

Deng, T., Wang, X.M., Ni, X.J., Liu, L.P., Liang, Z., 2004. Cenozoic stratigraphic sequence of the Linxia Basin in Gansu, China and its evidence from mammal fossils. Vertebr. Palasat. 42, 45–66 (in Chinese with English abstract).

Deng, T., Qiu, Z.X., Wang, B.Y., Wang, X.M., Hou, S.K., 2013a. Late Cenozoic biostratigraphy of the Linxia basin, northwestern China. In: Wang, X.M., Flynn, L.J., Fortelius, M. (Eds.), Fossil Mammals of Asia: Neogene Biostratigraphy and Chronology. Columbia University Press, New York, pp. 243–273.

Deng, T., Hou, S.K., Xie, G.P., Wang, S.Q., Shi, Q.Q., Chen, S.K., Sun, B.Y., Lu, X.K., 2013b. Chronostratigraphic subdivision and correlation of the upper Miocene of the Linxia Basin. J. Stratigr. 37, 417–427 (in Chinese with English abstract).

Deng, C.L., Hao, Q.Z., Guo, Z.T., Zhu, R.X., 2019a. Quaternary integrative stratigraphy and timescale of China. Sci. China Earth Sci. 62, 324–348.

Deng, T., Hou, S.K., Wang, S.Q., 2019b. Neogene integrative stratigraphy and timescale of China. Sci. China Earth Sci. 62, 310–323.

Dupont-Nivet, G., Hoorn, C., Konert, M., 2008. Tibetan uplift prior to the Eocene-Oligocene climate transition: evidence from pollen analysis of the Xining Basin. Geology 36, 987–990.

Fang, X.M., Li, J.J., Zhu, J.J., Chen, H.L., Cao, J.X., 1997. Absolute chronology and partition of the Cenozoic strata in the Linxia Basin, Gansu. Chin. Sci. Bull. 42, 1457–1471 (in Chinese with English abstract).

Fang, X.M., Garzione, C., Van der Voo, R., Li, J.J., Fan, M.J., 2003. Flexural subsidence by 29 Ma on the NE edge of Tibet from the magnetostratigraphy of Linxia Basin, China. Earth Planet. Sci. Lett. 210, 545–560.

Fang, X.M., Zhao, Z.J., Li, J.J., Yan, M.D., Pan, B.T., Song, C.H., Dai, S., 2004. The late Cenozoic magnetostratigraphy of the Laojunmiao anticline on the north margin of the Qilian Shan and uplift of the north Tibetan Plateau. Sci. China Earth Sci. 34, 97–106 (in Chinese with English abstract).

Fang, X.M., Wang, J., Zhang, W.L., Zan, J.J., Song, C.H., Yan, M., Appel, E., Zhang, T., Wu, F., Yang, Y., Lu, Y., 2016. Tectonosedimentary evolution model of an intracontinental flexural (foreland) basin for paleoclimatic research. Glob. Planet. Chang. 145, 78–97.

Garzione, C.N., Ikari, M.J., Basu, A.R., 2005. Source of Oligocene to Pliocene sedimentary rocks in the Linxia basin in northeastern Tibet from Nd isotopes: Implications for tectonic forcing of climate. Geol. Soc. Am. Bull. 117, 1156–1166.

Gansu Geological and Mineral Resources Bureau, 1989. In: Regional Geology of Gansu Province. Geological Publishing House, Beijing, pp. 1–100 (in Chinese).

Granger, D.E., 2006. A review of burial dating methods using 26Al and 10Be. Geol. Soc. Am. Spec. Pap. 415, 1–16.

Granger, D.E., 2014. Cosmogenic nuclide burial dating in archaeology and paleoanthropology. In: Turekian, K., Holland, H. (Eds.), Treatise on Geochemistry, second ed., Vol. 14. Elsevier Publishing, pp. 81–97.

Granger, D.E., Muzikar, P.F., 2001. Dating sediment burial with in situ-produced cosmogenic nuclides: theory, techniques, and limitations. Earth Planet. Sci. Lett. 188, 269–281.

Han, F., Chen, J., Yin, G.M., 2015. Cosmogenic nuclides 26Al/10Be burial dating of Xiyu conglomerate. Quat. Sci. 35, 109–117 (in Chinese with English abstract).

Heermance, R.V., Chen, J., Burbank, D.W., Wang, C.S., 2007. Chronology and tectonic controls of late Tertiary deposition in the southwestern Tian Shan foreland, NW China. Basin Res. 19, 599–632.

Hilgen, F.J., Iaccarino, S., Krijgsman, W., Villa, G., Langereis, C.G., Zachariasse, W.J., 2000. The Global boundary Stratotype Section and Point (GSSP) of the Messinian Stage (uppermost Miocene). Episodes 23, 172–178.
Hoorn, C., Straathof, J., Abels, H.A., Xu, Y., Utescher, T., Dupont-Nivet, G., 2012. A late Eocene palynological record of climate change and Tibetan Plateau uplift (Xining Basin, China). Palaeogeogr. Palaeoclimatol. Palaeoecol. 344–345, 16–38.
Huang, B.C., Piper, J.D.A., Qiao, Q.Q., Wang, H.L., Zhang, C.X., 2010. Magnetostratigraphic and rock magnetic study of the Neogene upper Yaha section, Kuche Depression (Tarim Basin): Implications to formation of the Xiyu conglomerate formation, NW China. J. Geophys. Res. 115, B01101.
Ji, J.L., Luo, P., White, P., Jiang, H.C., Gao, L., Ding, Z.L., 2008. Episodic uplift of the Tianshan Mountains since the late Oligocene constrained by magnetostratigraphy of the Jingou River section, in the southern margin of the Junggar Basin, China. J. Geophys. Res. Solid Earth 113, B05102.
Ji, J.L., Zhu, M., Wang, X., Luo, P., Dong, X.X., 2010. Ages of the Cenozoic strata on the southern margin of Junggar Basin, northwestern China. J. Stratigr. 34, 43–50 (in Chinese with English abstract).
Jing, X.H., Shen, Z.Y., Wang, X., Yu, Y.L., Pan, X.Q., 2011. Magnetostratigraphic construct of Awate section in the North Tarim Basin: the impulse uplift of Tianshan range. Chin. J. Geophys. 54, 334–342 (in Chinese with English abstract).
Kober, F., Alfimov, V., Ivy-Ochs, S., Kubik, P.W., Wieler, R., 2011. The cosmogenic 21Ne production rate in quartz evaluated on a large set of existing 21Ne-10Be data. Earth Planet. Sci. Lett. 302, 163–171.
Kohl, C.P., Nishiizumi, K., 1992. Chemical isolation of quartz for measurement of in–situ-produced cosmogenic nuclides. Geochem. Cosmochim. Acta 56, 3583–3587.
Kong, P., Zheng, Y., Fu, B.H., 2011. Cosmogenic nuclide burial ages and provenance of late Cenozoic deposits in the Sichuan Basin: Implications for early Quaternary glaciations in East Tibet. Quat. Geochronol. 6, 304–312.
Lal, D., 1991. Cosmic ray labeling of erosion surfaces: in situ nuclide production rates and erosion models. Earth Planet. Sci. Lett. 104, 424–439.
Li, C.X., Dupont-Nivet, G., Guo, Z.J., 2011. Magnetostratigraphy of the northern Tian Shan foreland, taxi he section, China. Basin Res. 23, 101–117.
Li, J.J., 1991. The environmental effects of the uplift of the Qinghai-Xizang Plateau. Quat. Sci. Rev. 10, 479–483.
Li, J.J., et al., 1995. In: Uplift of Qinhai-Xizang (Tibet) Plateau and Global Change. Lanzhou University Press, Lanzhou, pp. 1–207 (In Chinese).
Li, J.J., Wen, S.X., Zhang, Q.S., Wang, F.B., Zhen, B.X., Li, B.Y., 1979. Discussion on the uplift age, extent and forms of the Tibetan Plateau. Sci. China 6, 608–616 (in Chinese with English abstract).
Li, J.J., Fang, X.M., Ma, H.Z., Zhu, J.J., Pan, B.T., Chen, H.L., 1996. Geomorphologic and environmental evolution in the upper reaches of the Yellow River during the Late Cenozoic. Sci. China Ser. D Earth Sci. 39, 380–390.
Li, J.J., Fang, X.M., Van der Voo, R., Zhu, J.J., Mac Niocaill, C., Cao, J.X., Zhong, W., Chen, H.L., Wang, J.L., Wang, J.M., Zhang, Y.C., 1997. Late Cenozoic magnetostratigraphy (11–0 Ma) of the Dongshanding and Wangjiashan sections in the Longzhong Basin, western China. Geol. Mijnb. 76, 121–134.
Li, Y., Densmore, A.L., Zhou, R.J., Ellis, M.A., Zhang, Y., Li, B., 2006. Profiles of digital elevation models crossing the eastern margin of the Tibetan Plateau and their constraints on dissection depths and incision rates of late Cenozoic rivers. Quat. Sci. 26, 236–243 (in Chinese with English abstract).
Liu, D.L., Song, C.H., Yan, M.D., Zhang, W.L., Fang, X.M., Li, H.B., 2011. Preliminary study on the tempral and spatial variations of sedimentation rates of the Yumen conglomerate and its implications for climate-tectonics interaction. Geotecton. Metallog. 35, 56–63 (in Chinese with English abstract).
Liu, P., Zhang, S., Han, J.M., Liu, T.S., 2008. Paleomagnetic chronology of Quaternary stratigraphy of the Longdan section in Gansu Province of China. Quat. Sci. 28 (5), 796–805 (in Chinese with English abstract).
Liu, P., Deng, C.L., Li, S.H., Cai, S.H., Cheng, H.J., Yuan, B.Y., Wei, Q., Zhu, R.X., 2012. Magnetostratigraphic dating of the Xiashagou Fauna and implication for sequencing the mammalian faunas in the Nihewan Basin, North China. Palaeogeogr. Palaeoclimatol. Palaeoecol. 315–316, 75–85.
Ma, W.Z., 2007. Tectonic significance of sedimentary record in northern edge of Altyn Tagh range (M.Sc. thesis). In: Lanzhou University, Lanzhou, pp. 1–80.
Ma, Y., Wu, Y., Li, D., Zheng, D., 2015. Analytical procedure of neon measurements on GV 5400 noble gas mass spectrometer and its evaluation by quartz standard CREU-1. Int. J. Mass Spectrom. 380, 26–33.
Ma, Y., Wang, W.T., Zheng, D.W., Zhang, H.P., Pang, J.Z., Wu, Y., Stuart, F.M., Xu, S., 2018. Mid-Miocene cosmogenic upper limit for 10Be/21Ne burial age. Quat. Geochronol. 48, 72–79.
Miao, Y.F., Wu, F.L., Herrmann, M., Yan, X.L., Meng, Q.Q., 2013. Late early Oligocene East asian summer monsoon in the NE Tibetan Plateau: evidence from a palynological record from the Lanzhou Basin, China. J. Asian Earth Sci. 75, 46–57.
Molnar, P., England, P., 1990. Late Cenozoic uplift of mountain ranges and global climate change: chicken or egg? Nature 346, 29–34.
Molnar, P., England, P., Martinod, J., 1993. Mantle dynamics, the uplift of the Tibetan Plateau, and the indian monsoon. Rev. Geophys. 31, 357–396.
Nakayama, K., Ulak, P.D., 1999. Evolution of fluvial style in the siwalik Group in the foothills of the Nepal Himalaya. Sediment. Geol. 125, 205–224.
Ogg, J.G., 2020. Geomagnetic polarity time scale. In: Gradstein, F.M., Ogg, J.M., Schmitz, M.D., et al. (Eds.), Geologic Time Scale 2020, Vol. 1. Elsevier, Amsterdam, pp. 159–192.
Qiao, Q.Q., Huang, B.C., Biggin, A.J., Piper, J.D.A., 2017. Late Cenozoic evolution in the Pamir-Tian Shan convergence: new chronological constraints from the magnetostratigraphic record of the southwestern Tianshan foreland basin (Ulugqat area). Tectonophysics 717, 51–64.
Qiu, Z.X., Qiu, Z.D., 1995. Chronological sequence and subdivision of Chinese Neogene mammalian faunas. Palaeogeogr. Palaeoclim. Palaeoecol. 116, 41–70.
Qiu, Z.X., Wu, W.Y., Qiu, Z.D., 1999. Miocene mamal faunal sequence of China: palaeozoogeography and Eurasian relationships. In: Rössner, G.E., Heissig, K. (Eds.), The Miocene Land Mammals of Europe. Verlag Dr. Friedrich Pfeil, Münehen, pp. 443–455.
Qiu, Z.X., Deng, T., Wang, B.Y., 2004. Early Pleistocene mammalian fauna from Longdan, Dongxiang, Gansu, China. In: Palaeont. Sin. New Ser. C, No. 27 (Whole No. 191). Science Press, Beijing, pp. 157–193 (in Chinese with English summary).
Qiu, Z.X., Wang, B.Y., Deng, T., 2004a. Mammal fossils from Yagou, Linxia Basin, Gansu, and related stratigraphic problems. Vertebr. PalSiat. 42, 276–296 (in Chinese with English abstract).
Sinha, R., Kumar, R., Sinha, S., Tandon, S.K., Gibling, M.R., 2007. Late Cenozoic fluvial successions in northern and western India: an overview and synthesis. Quat. Sci. Rev. 26, 2801–2822.
Singer, B.S., 2014. A Quaternary geomagnetic instability time scale. Quat. Geochronol. 21, 29–52.
Singer, B.S., Jicha, B.R., Condon, D.J., Macho, A.S., Hoffman, K.A., Dierkhising, J., Brown, M.C., Feinberg, J.M., Kidane, T., 2014. Precise ages of the Réunion event and Huckleberry Ridge excursion: Episodic clustering of geomagnetic instabilities and the dynamics of flow within the outer core. Earth Planet. Sci. Lett. 405, 25–38.
Stone, J., 2000. Air pressure and cosmogenic isotope production. J. Geophys. Res. 105, 23753–23759.
Sun, J.M., Zhu, R.X., Bowler, J., 2004. Timing of the Tianshan Mountains uplift constrained by magnetostratigraphic analysis of molasse deposits. Earth Planet. Sci. Lett. 219, 239–253.
Sun, J.M., Zhang, Z.Q., 2009. Syntectonic growth strata and implications for late Cenozoic tectonic uplift in the northern Tian Shan, China. Tectonophysics 463, 60–68.
Sun, J.M., Liu, T.S., 2006. The age of the Taklimakan Desert. Science 312, 1621.
Sun, J.M., Xu, Q.H., Huang, B.C., 2007. Late Cenozoic magnetochronology and paleoenvironmental changes in the northern foreland basin of the Tian Shan Mountains. J. Geophys. Res. Solid Earth 112, B04107.
Sun, J.M., Li, Y., Zhang, Z.Q., Fu, B., 2009. Magnetostratigraphic data on Neogene growth folding in the foreland basin of the southern Tianshan Mountains. Geology 37, 1051–1054.
Sun, L., Deng, C.L., Deng, T., Kong, Y.F., Wu, B.L., Liu, S.Z., Li, Q., Liu, G., 2023. Magnetostratigraphy of the Oligocene and Miocene of the Linxia Basin, northwestern China. Palaeogeogr. Palaeoclimatol. Palaeoecol. 613, 111404 https://doi.org/10.1016/j.palaeo.2023.111404.
Sun, L., Deng, C.L., Wang, X.M., Li, Q., Qin, H.F., Xu, H.R., Kong, Y.F., Wu, B.L., Liu, S.Z., Zhu, R.X., 2018. Magnetostratigraphic dating of the late Miocene Baogeda Ula Formation and associated fauna in Central Inner Mongolia, northern China. Palaeogeogr. Palaeoclimatol. Palaeoecol. 505, 243–255.
Sun, L., Deng, C.L., Hao, Q.Z., Liu, C.C., Yi, L., Liu, P., Gao, X.B., Xiong, J.G., Yang, S.X., Ge, J.Y., 2021. Lithostratigraphic subdivision and correlation of the Quaternary in China. J. Stratigr. 45, 440–459 (in Chinese with English abstract).
Tapponnier, P., Xu, Z.Q., Roger, F., Meyer, B., Arnaud, N., Wittlinger, G., Yang, J.S., 2001. Oblique stepwise rise and growth of the Tibet Plateau. Science 294, 1671–1677.
Tu, H., Luo, L., Deng, C.L., Ou, Z.L., Lai, Z.P., Shen, G.J., Bae, C.J., Granger, D., 2022. Isochron 26Al/10Be burial dating of the Xiashagou Fauna in the Nihewan Basin, northern China: Implications for biogeography and early hominin dispersals. Quat. Sci. Rev. 283, 107447.
Vermeesch, P., Balco, G., Blard, P.H., Dunai, T., Kober, F., Niedermann, S., Shuster, D.L., Strasky, S., Stuart, F.M., Wieler, R., Zimmermann, L., 2015. Interlaboratory comparison of cosmogenic 21Ne in quartz. Quat. Geochronol. 26, 20–28.
Wang, S.L., Li, Y., Li, Y.Z., Zhang, Y.X., 2003. Sedimentary characteristics of the Cenozoic Dayi conglomerate in Chengdu Basin. J. Chengdu Univ. Technol. 30, 139–146 (in Chinese with English abstract).
Xu, S., Freeman, S., Rood, D.H., Shanks, R.P., 2015. Decadal 10Be, 26Al and 36Cl QA measurements on the SUERC 5MV accelerator mass spectrometer. Nucl. Inst. Methods Phys. Res. B 361, 39–42.
Yang, S.L., Ding, Z.L., 2010. Drastic climatic shift at ~2.8 Ma as recorded in eolian deposits of China and its implications for redefining the Pliocene-Pleistocene boundary. Quat. Int. 219 (1–2), 37–44.
York, D., Evensen, N.M., Martinez, M.L., Delgado, J.D.B., 2004. Unified equations for the slope, intercept, and standard errors of the best straight line. Am. J. Phys. 72, 367–375.
Yuan, J., Deng, C.L., Yang, Z.Y., Krijgsman, W., Qin, H.F., Shen, Z.S., Hou, Y.F., Zhang, S., Yu, Z.Q., Zhao, P., Zhao, L., Wan, B., He, H.Y., Guo, Z.T., 2022. Triple-stage India-Asia collision involving arc-continent collision and subsequent two-stage continent-continent collision. Glob. Planet. Change 212, 103821.
Zan, J.B., Fang, X.M., Zhang, W.L., Yan, M.D., Zhang, T., 2016. Palaeoenvironmental and chronological constraints on the early Pleistocene mammal fauna from loess deposits in the Linxia Basin, NE Tibetan Plateau. Quat. Sci. Rev. 148, 234–242.
Zan, J.B., Fang, X.M., Li, X.J., Zhang, W.L., Yan, M.D., Shen, M.M., 2018. Late Pliocene monsoonal gradients in Western China recorded by the eolian deposits from the Linxia Basin, NE Tibetan Plateau. J. Geophys. Res. Atmos. 123, 8047–8061.
Zhao, Z.J., Granger, D.E., Chen, Y., Shu, Q., Liu, G.F., Zhang, M.H., Hu, X.F., Wu, Q.L., Hu, E.Y., Li, Y., Yan, Y.J., Qiao, L.L., 2017. Cosmogenic nuclide burial dating of an alluvial conglomerate sequence: an example from the Hexi Corridor, NE Tibetan Plateau. Quat. Geochronol. 39, 68–78.
Zhang, P.Z., Molnar, P., Downs, W.R., 2001. Increased sedimentation rates and grain sizes 2–4 Myr ago due to the influence of climate change on erosion rates. Nature 410, 891–897.

Zhang, T., Fang, X.M., Song, C.H., Appel, E., Wang, Y.D., 2014. Cenozoic tectonic deformation and uplift of the South Tian Shan: Implications from magnetostratigraphy and balanced cross-section restoration of the Kuqa depression. Tectonophysics 628, 172–187.

Zhang, W.L., Appel, E., Wang, J.Y., Fang, X.M., Zan, J.B., Yang, Y.B., Miao, Y.F., Yan, X. L., 2019. New paleomagnetic constraints for Platybelodon and Hipparion faunas in the Linxia Basin and their ecological environmental implications. Glob. Planet. Chang. 176, 71–83.

Zhang, W.L., Fang, X.M., Song, C.H., Yan, M.D., Wang, J.Y., Zhang, Z.G., Wu, F.L., Zan, J. B., Zhang, T., Yang, Y.B., Tan, M.Q., 2020. Magnetostratigraphic constraints on the age of the Hipparion fauna in the Linxia Basin of China, and its implications for stepwise aridification. Palaeogeogr. Palaeoclimatol. Palaeoecol. 537, 109413.

Zheng, D.W., Zhang, P.Z., Wan, J.L., Yuan, D.Y., Li, D.M., Wang, J.P., Yin, J.W., Li, C.Y., Wang, Z.C., 2006. Tectonic events climate and conglomerate: example from Jishishan Mountain and Linxia Basin. Quat. Sci. 26, 63–69 (in Chinese with English abstract).

Zheng, H.B., Huang, X.T., Butcher, K., 2006. Lithostratigraphy, petrography and facies analysis of the late Cenozoic sediments in the foreland basin of the West Kunlun. Palaeogeogr. Palaeoclimatol. Palaeoecol. 241, 61–78.

Zheng, Y., Qiu, Z.X., Qiu, Z.D., Li, L., Wei, X.H., Zhang, R., Yue, L.P., Deng, T., 2023. Revised magnetostratigraphy of the Linxia Basin in the northeast Tibetan Plateau, constrained by micromammalian fossils. Palaeogeogr. Palaeoclimatol. Palaeoecol. 623, 111620.